Scalable projected Light Sheet Microscopy for high-resolution imaging of large samples

Yannan Chen[1,2], Cheng Gong[1,2], Shradha Chauhan[1], Estanislao Daniel De La Cruz[1], Malika S. Datta[1,3], Raju Tomer[1,2,3,*]

[1]Department of Biological Sciences

[2]Department of Biomedical Engineering

[3]Mortimer B. Zuckerman Mind Brain and Behavior Institute

Columbia University

*Corresponding author, Lead Contact: raju.tomer@columbia.edu

Abstract

Light sheet fluorescence microscopy (LSFM) is a highly effective imaging technique used for live and fixed samples, particularly for high-resolution mapping of large cleared intact organs. However, existing high-performance LSFM implementations are often prohibitively expensive and lack scalability needed for high-throughput applications. Here, we introduce a low-cost and scalable framework, called projected Light Sheet Microscopy (pLSM), which repurposes readily available off-the-shelf consumer-grade components, incorporates optimized optical paths and employs an over-the-network control architecture to achieve high-resolution imaging of large samples. We comprehensively characterize the pLSM framework and demonstrate its capabilities in high-resolution, multi-color imaging of intact mouse brains and post-mortem human brain samples cleared using various methods. Furthermore, we demonstrate the potential of pLSM-generated data for comprehensive phenotyping of the entire brain by mapping the distribution of dopaminergic neurons and microvasculature architecture throughout the brain. The pLSM framework has the potential to further democratize LSFM and facilitate greater scalable access to high-resolution light sheet microscopy.

INTRODUCTION

Light sheet fluorescence microscopy (LSFM) has emerged as a powerful and versatile approach for biological imaging, enabling prolonged *in vivo* observations and facilitating high-resolution imaging of large cleared intact organs[1]. These remarkable capabilities are achieved through LSFM's distinctive orthogonal planar illumination and detection geometry, which minimizes energy load and allows use of fast CMOS camera-based wide-field detection. In recent years, several highly optimized LSFM implementations have been developed for high-speed phenotyping of intact cleared organs at high resolution[1–10]. However, the substantial costs associated with implementing these systems and their limited scalability hinder their utility in high-throughput imaging applications and impede broader accessibility within the scientific community. To address some of these constraints, several open-source initiatives have emerged, including openSPIM[11], OpenSpinMicroscopy[12] and mesoSPIM[13], which aim to optimize the cost and portability of LSFM. Nevertheless, there is still an unmet need for further cost-optimized implementations and genuinely scalable systems that can operate remotely over networks to facilitate high-throughput applications such as drug screening and the characterization of diseased brains.

In this study, we present a novel LSFM imaging framework called projected LSFM (pLSM), which offers a highly cost-optimized and scalable solution while maintaining excellent imaging quality. Our approach leverages off-the-shelf components, including pocket LASER projectors as multi-color illumination sources, Nvidia Jetson Nano boards for electronic control, 3D-printed imaging chambers, and optimized scan and detection optics. Additionally, we have developed a network-based imaging workflow using native Python and Jupyter Notebook, enabling remote control of multiple microscopes at scale. In our extensive characterization of the pLSM system, we demonstrate its robustness and versatility by performing high-resolution multi-color imaging of large mouse and human brain samples cleared using various methods. Moreover, we showcase the system's capabilities in whole-brain quantitative phenotyping, revealing insights comparable to those obtained from high-end LSFM systems. Through the incorporation of readily available consumer-grade components and a network-based imaging workflow, pLSM provides a cost-effective, scalable, and high-resolution imaging solution for large biological samples, democratizing LSFM and making it suitable for a wide range of high-throughput applications.

RESULTS

pLSM implementation

The LSFM system encompasses orthogonal illumination and detection optics, laser light sources, control electronics, and data acquisition software[1]. Our goal was to optimize the cost-effectiveness of each component by incorporating readily available, low-cost consumer-grade parts, while ensuring high imaging

quality. The pLSM system comprises two identical modules for light-sheet illumination, which collectively provide comprehensive coverage of large cleared samples, along with an orthogonal wide-field detection arm for image detection (**Fig. 1a-b**, **Supplementary Table 1**). Additionally, 3D motorized stages are employed for multi-tile imaging of large samples mounted in quartz glass cuvettes[2,3] within a 3D-printed immersion chamber. To implement the electronic controls and imaging workflow, we employed a cost-effective Nvidia Jetson Nano board, which can be operated remotely via an SSH-based connection and a Python-based control software GUI within the Jupyter Notebook framework (**Fig. 1c**).

For the detection arm, we utilized a long-working distance air objective (Mitutoyo 10x Plan Apo), a 200 mm focal length tube lens (TTL-200, Thorlabs), a multi-band pass emission filter, and a low-cost consumer-grade CMOS camera (GS3-U3-89S6M-C, FLIR, 3.45 µm pixel) for wide-field detection of the illuminated plane. Notably, this camera provided performance comparable to high-end sCMOS camera, albeit with lower quantum efficiency. Next, we sought to develop cost-effective alternatives to expensive multi-laser engines, galvo scanners, and associated controllers for generation of thin illumination light sheets. To achieve this, we devised an approach that employs pocket laser projectors for generation of high-quality scanned light sheets with 3-color imaging capabilities (**Fig. 1**). We found that these economical projectors provide substantial benefits of fully integrated 3-color laser diodes (TO-8 set with blue: 440-460 nm, green: 515-530 nm, and red: 632-642 nm) with sufficient power needed for imaging, MEMS 2D-scanners, and associated electronics in a compact assembly. However, adapting them for light-sheet generation presented practical challenges in controlling the various light-sheet properties, positioning, and scanning speeds. To address these challenges, we devised a control framework utilizing the Python X library (Python-Xlib) to directly modulate various scanning parameters (**Fig. 1c**). This framework allows the generation of light sheets as multi-pixel (1 or more, on-demand) wide projected lines of specific height and location (**Fig. 2a-d**). Importantly, this approach also offers the unique advantage of easily modulating the light sheet's thickness and field-of-view (FOV) by controlling the pixel widths of the projected line (**Fig. 2d**). Downstream to the projector, we employed a Plössl lens (implemented as a pair of achromats, AC254-045-A) as an effective substitute for expensive f-theta scan lenses, an achromat doublet (AC508-075-A) as a tube lens, and an air illumination objective (Mitutoyo 10x Plan Apo).

The pLSM control framework and imaging workflows were implemented on a cost-effective Nvidia Jetson Nano board running the Linux operating system. The Spinnaker SDK package for image grabbing and Python-Xlib for light sheet projection. The acquired images are streamed to a USB 3.0 high-speed solid-state hard drive. The control GUI was implemented using IPyWidgets within the Jupyter Notebook framework, enabling remote operation via a SSH connection from any machine. This network-controlled framework allows for easy scalability without requiring the full capacity of a remote machine.

pLSM characterization

We first performed a comprehensive characterization of the light sheets generated through the utilization of multi-pixel projected lines in our pLSM framework. We imaged micron-size fluorescent beads to characterize the light sheet and detection point spread functions. As shown in **Fig. 2c-d**, in this implementation of the pLSM, the generated light sheets have a thickness of ~5 μm when using a single pixel projected line. Furthermore, for larger pixel widths projected lines, we observed sub-linear increases in the thickness of the light sheet (**Fig. 2d**). Importantly, the modulation of light sheet thickness and field-of-view can be easily accomplished at the software level, offering a convenient means for rapid adaptation to diverse experimental requirements. Additionally, our findings indicate that this approach yields a flatter intensity profile across the light sheet cross-section compared to a standard Gaussian light sheet of similar thickness (**Fig**. **2b-d**). Notably, the scanning speed of the light sheet, and consequently the imaging speed, is solely determined by the projector refresh rate (60 Hz for the utilized model), independent of the pixel widths employed. As a result, pLSM presents a highly adaptable multi-scale scheme capable of accommodating various imaging needs, spanning from high axial resolution settings to high-volume acquisition rates with thicker light sheets.

To further evaluate the imaging performance of pLSM, we conducted a direct comparison with a high-end COLM[2,3] system. To this end, we utilized the same cleared mouse brain sample stained for dopaminergic neurons and acquired images using both pLSM and COLM implementations. Quantification of the intensity distribution, as presented in **Fig 2e-f**, demonstrates that pLSM achieves imaging quality comparable to that of the high-end COLM implementation. This result highlights the capabilities of pLSM in delivering high-resolution imaging outcomes on par with established state-of-the-art methodologies. Furthermore, we demonstrate the multi-color imaging capability of pLSM by performing 2-channel imaging of a post-mortem human brain sample stained with two different markers of vasculatures **(Fig. 2g)** by using green (515-530 nm) and red (632-642 nm) light. Overall, pLSM allows high-resolution imaging of biological samples with comparable quality to high-end implementations.

In summary, the detailed characterization demonstrates that pLSM provides high-quality imaging comparable to high-end and expensive LSFM implementations, while offering a flexible, cost-effective, and scalable platform for high-resolution imaging of biological samples.

High-resolution mapping of large intact samples cleared with multiple clearing methods

To facilitate the imaging of large cleared samples, we optimized the pLSM imaging workflow to address sample-induced optical aberrations at different positions. A crucial improvement involves the implementation of a linearly adapting light-sheet offset correction procedure. This procedure compensates

for misalignments in the light sheet and detection focal plane caused by optical property changes within a large sample. By sampling optimal parameters at a few anchor positions and applying linear interpolation within the convex hull of these points, we generate smoothed light-sheet offsets. This adaptive offset parameter correction enables high-quality imaging by compensating for the optical shifts resulting from refractive index mismatches. Moreover, it ensures the compatibility of pLSM with various tissue clearing methods.

To demonstrate the capabilities of pLSM, we conducted high-resolution imaging of intact mouse brain samples that were cleared using the iDISCO[14] and CLARITY[2,15] methods. In one experiment, we focused on the whole-brain mapping of the dopamine (DA) system using pLSM imaging. The intact mouse brain samples were stained with an antibody against tyrosine hydroxylase (TH), a widely used marker of DA neurons, and an Alexa Fluor 647 secondary antibody to label the entire dopamine system. Following staining, the samples were cleared using the iDISCO method and mounted in a quartz glass cuvette for imaging with red projected lines (632-642 nm) and a 577/690 band-pass emission filter. As shown in **Fig. 3a** and **Supplementary videos 1-2**, pLSM successfully achieved comprehensive imaging of the intact mouse brain sample with high imaging quality, allowing for complete reconstruction of the mouse dopamine system. The imaging results obtained were comparable to those achieved by high-end implementations (**Supplementary video 2**).

Furthermore, we employed pLSM for high-resolution mapping of the entire vasculature in the intact mouse brain. To this end, we utilized a cocktail of antibodies against Podocalyxin, CD31, and Acta2, all detected using the same Alexa 647 secondary antibody, similar to a previous report[16]. The labeled samples were cleared using the iDISCO protocol and imaged using a red-color (632-642 nm) projected light sheet and an Edmund 577/690 emission filter. As demonstrated in **Fig. 3b**, pLSM enabled imaging of the entire vasculature in the intact mouse brain sample.

Moreover, to demonstrate the compatibility of pLSM with different tissue clearing methods, we performed whole-brain imaging of CLARITY-cleared mouse brain samples from the *Thy1-eYFP* transgenic mouse line. The samples were cleared using the passive CLARITY method[2] and mounted in quartz glass cuvettes for imaging with green-color (515-530 nm) projected lines and an Edmund 577/690 emission filter. As shown in **Fig. 3c**, pLSM successfully achieved high-resolution imaging of the entire intact brain.

Overall, these imaging experiments substantiate the capability of pLSM for high-resolution imaging of large intact samples that have been cleared using multiple methods. The incorporation of the linearly adapting light-sheet offset correction procedure addresses optical aberrations, ensuring high quality imaging throughout the sample.

Compatibility of pLSM datasets with whole brain analysis

We aimed to investigate whether the whole brain datasets acquired using the pLSM system could yield quantitative insights comparable to those obtained from high-end LSFM implementations. To address this, we conducted high-resolution imaging of a whole brain sample with labeled dopamine (DA) neurons using both pLSM and the COLM system (**Fig. 4**, **Supplementary Video 3**). Subsequently, we utilized our recently developed suiteWB pipeline[17], a high-accuracy whole brain phenotyping framework, to detect TH+ DA neurons and map their brain-wide distributions by aligning the data with the Allen Brain Atlas (ABA) annotations. In brief, the suiteWB pipeline aligned the whole brain dataset to a local average reference brain with annotated regions based on ABA. The detection of DA neurons was performed using a multi-model segmentation approach of separate processing of regions with sparse and high DA neuron densities, which were then merged to generate whole brain point clouds. By directly comparing the point clouds generated from the pLSM and COLM acquired datasets from same sample (**Fig. 4**, **Supplementary Video 3**), we observed strong agreements across all brain regions. This rigorous quantitative analysis demonstrates the compatibility of pLSM-acquired data with whole brain analysis approaches, facilitating the generation of detailed brain-wide maps.

In conclusion, these findings indicate that the pLSM system, despite its cost-effective nature, is capable of producing quantitative insights comparable to those obtained from high-end LSFM systems when analyzing whole brain datasets. This highlights the robustness and reliability of pLSM in providing accurate and comprehensive information for investigating complex biological processes at the whole organ level.

DISCUSSION

In this study, we introduced a novel LSFM imaging framework called pLSM, which offers a highly cost-optimized and scalable solution for high-resolution imaging of large intact biological samples. By leveraging off-the-shelf components, including inexpensive pocket LASER projectors and Nvidia Jetson Nano boards, the pLSM implementation costs are significantly reduced, making it a cost-effective alternative to high-end LSFM systems. In addition to hardware component optimization, a key feature of the pLSM system is the implementation of a Jupyter notebook-based operation of imaging workflows. This control architecture enables remote control of the system through an interactive and user-friendly interface, facilitating the operation of multiple microscopes simultaneously. The network-based approach also simplifies the deployment of the system, promoting collaboration and remote access to the high-resolution imaging.

We demonstrated the robustness and versatility of the pLSM framework through extensive optical characterization (**Fig. 2**) and imaging of diverse samples, including intact mouse brains and post-mortem human brain tissues cleared with multiple tissue clearing methods (**Fig. 2-4**). The imaging performance of pLSM was found to be comparable to the high-end implementations. Importantly, we showed that the cost-effective nature of the pLSM framework did not compromise its compatibility with the whole brain analysis approaches to yield brain-wide quantitative insights at high resolution. While the imaging quality is a crucial aspect of LSFM systems, the imaging speed also plays a significant role. In the pLSM system, we capitalized on the fast refresh rate of the pocket LASER projectors and utilized the Xlib library for efficient light sheet scanning, resulting in high-speed imaging capabilities. However, it is important to note that the scanning speeds achieved using pocket LASER projectors may not reach the levels afforded by fast resonant galvo scanners. Future enhancements could involve the integration of more advanced projectors to further boost imaging speed.

Overall, the pLSM system represents a significant advancement in democratizing LSFM technology. By reducing implementation costs and maintaining high imaging quality, pLSM opens up new possibilities for high-throughput imaging applications, including drug screening and characterization of diseased brains. The incorporation of off-the-shelf components and a network-based imaging workflow further contributes to the system's scalability. In conclusion, pLSM provides a cost-effective, scalable, and high-resolution imaging solution for large biological samples, enabling broader access to LSFM technology and its potential applications.

METHODS

***pLSM setup*.** The pLSM system consists of two illumination and one detection arms (**Fig. 1**), mounted on 60 mm cage assembly system (Thorlabs) (**Supplementary Table 1** lists all components). Each illumination arm utilizes a MEMS LASER projector (Nebra Anybeam), mounted on two dovetail translation stages (DT12) for precise adjustment along the light path. The projector incorporates TO-8 LASER diodes that provide blue (440-460nm), green (515-530nm), and red (632-642nm) colors. A combination of two achromatic doublets (AC254-045-A) forms a Plössl-style scan lens with a focal length of approximately 22.5mm. An achromat doublet (AC508-075-A) was paired with an air objective (Mitutoyo 10x Plan Apo) for illumination. In the detection arm, the same objective (Mitutoyo 10x Plan Apo) is used, along with a tube lens (TTL200) and a CMOS camera (GS3-U3-89S6M-C, FLIR) with a pixel dimension of 3.45 µm. A multi-band filter (577/690nm, #87-251, Emund Optics or 432/515/595/730 nm, Semrock) was used as the emission filter. To match refractive index, a custom-designed oil chamber is 3D printed using polylactic acid (PLA) and features windows for illumination and detection, sealed with cover glass (VWR). A refractive index matching oil with an RI of 1.454 (Cargille) is used to fill the chamber. Sample positioning

is achieved using a motorized stage (PT3 Z8, Thorlabs) for fine adjustments during imaging, along with additional 3-degree-of-freedom dovetail translation stages (DT12XYZ, Thorlabs) and a rotation stage (QRP02, Thorlabs) for additional flexibility during sample mounting. The sample is mounted in a quartz glass cuvette (FireflySci). The imaging workflow is implemented on Nvidia Jetson Nano board, which provides four high-speed USB 3.0, one HDMI, one DP, and one Ethernet ports. The HDMI ports of the two projectors are connected to the board's HDMI and DP display ports using an HDMI-HDMI cable and an active DP to HDMI cable, respectively. The projectors are powered through USB using Micro USB cables connected to two USB ports on the board. The camera is connected to the board's third USB port via a USB Micro B to USB Type A cable. A solid state hard drive is connected to the fourth USB port using a USB Type-C to USB cable. The board is connected to the control computer via an Ethernet cable for remote control. The motorized stages are connected to motor control boxes (KDC 101), which are then connected to the control computer.

pLSM control. The control software, implemented in Python, comprises several classes that handle different aspects of the system: (a) the Illumination Class controls the light sheet using the Xlib protocol to adjust the projector output, enabling precise control over the illumination settings; (b) the Camera Class utilizes the Spinnaker package to control the FLIR camera, allowing for parameter configuration and imaging trigger control; (c) the Widget Class is responsible for creating the software's graphical user interface (GUI) using the IPyWidgets package, providing an interactive control interface for the user; (c) the Experiment Class is responsible for setting all the experiment parameters, executing actions, and saving acquired images directly to the hard drive via USB 3.0. It coordinates the entire imaging process. Remote control of the software on the Nvidia Jetson Nano board is achieved through SSH protocol for secure remote access. The control GUI can be accessed through a web browser, providing convenience and flexibility in controlling the pLSM system remotely. For precise control of the motorized stage, the thorlabs_apt Python package was utilized. The motorized stage's movement is synchronized with the camera acquisition through the Experiment Class, ensuring precise alignment and coordination during the imaging process.

Brain samples. For mouse dopamine and vasculature labeling, CD1 WT (Crl:CD1(ICR), charles river #022) mice were used. *Thy1-eYFP* (B6.Cg-Tg(Thy1-YFP)HJrs/J, JAX Strain 003782) mice were used for the CLARITY sample. All experiments were performed with 8-10 weeks old mice. For the human vasculature samples, post-mortem frozen de-identified human cortex sample was used. All experimental procedures were approved by the IACUC at Columbia University.

Tissue fixation. The mouse brains were perfused with 4% PFA and extracted, followed by overnight fixation in 4% PFA at 4°C. Freshly frozen human brain samples were incubated in 4% PFA for one day at 4°C. All samples were washed and stored in 1xPBS at 4°C.

iDISCO sample preparation. Standard iDISCO[14] procedure was used, consisting of sample pretreatment, immunolabeling and clearing steps. For pretreatment, brain samples were dehydrated in 20%, 40%, 60%, 80%, 100%, 100% v/v methanal/H_2O series for 1h each, followed by 66% v/v dichloromethane (DCM)/methanal incubation overnight. The samples were then washed by 100% methanal 1h twice and incubated in 5% H_2O_2 v/v in deionized water overnight at 4°C. Then rehydration was performed in 80%, 60%, 40%, 20% v/v methanal/H_2O and PBS for 1h each. Before immunolabeling, the brain samples were first washed in PBS+0.2% Triton 1h for twice, followed by permeabilization in PBS+0.2% Triton at 37°C for 1 day. The samples were then blocked in 1% BSA in PBS for 1 day at 37°C. Antibody labelings were performed in PBS with 0.1% Triton / 1% BSA and corresponding primary antibodies. Anti-TH antibody (ab113, Abcam) was used at 1:500 dilution. The mouse brain vasculature labeling was performed similar to previously reported procedure[16], by using a cocktail of antibodies: goat anti-podocalyxin (1:1500, AF1556, R&D Systems), goat anti-CD31 (1:300, AF3628, R&D Systems) and rabbit anti-Acta2 (1:1000, ab21027, Abcam). Human vasculature labeling was performed by using a cocktail of goat anti-podocalyxin (1:20, AF1658, R&D Systems), mouse anti-CD31 (1:50, BBA7, R&D Systems) and rabbit anti-Acta2 (1:1000, ab21027, Abcam). The brain samples were incubated in primary labeling solution for 10 days at 37°C, with one solution replacement at the end of day 5. The brains were washed in PBS + 0.1% Triton for 5 times at least 1h each and until the next day. For the mouse TH labeling, donkey anti-sheep Alexa 647 (1:1000, A-21448, Thermofisher) was used; for mouse vasculature labeling, donkey anti-goat Alexa 647 (1:500, A-21447, Thermofisher) and donkey anti-rabbit Alexa 647 (1:500, A-32795, Thermofisher) were used. For human vasculature labeling, donkey anti-goat Alexa 647 (1:500, A-21447, Thermofisher), donkey anti-mouse Alexa 647 (1:500, A-32787, Thermofisher) and donkey anti-rabbit Alexa 555 (1:500, A-31572, Thermofisher) were used. Secondary antibody incubation was also done for 10 days at 37°C, with one solution replacement at the end of day 5. For clearing, samples were dehydrated in 20%, 40%, 60%, 80%, 100%, 100% v/v methanal/H_2O for 1h each step followed by incubation in 66% v/v DCM/methanal for 3h. The samples were then washed in DCM 15min twice and put in dibenzyl ether (DBE, 33630, Sigma-Aldrich, RI=1.562) for refractive index matching until the next day for imaging.

Thy1-eYFP CLARITY sample preparation. PFA fixed brain samples were incubated in 1% hydrogel monomers (HMs) consisting of 1% w/v acrylamide (#1610140, BioRad), 0.05% w/v bisacrylamide (#1610142, BioRad), 4% paraformaldehyde (15710-S, Electron Microscopy Sciences), 1xPBS, deionized water, and 0.25% of thermal initiator (VA-044, Fisher Scientific) at 4°C overnight followed by oxygen removal and replacement of nitrogen using vacuum pump. The air-tight sample was then polymerized at 37°C for 6 hours. Then the sample was undergone passively clearing by incubating in SBC buffer at 37°C with gentle shaking. Sample transparency was assessed to determine clearing completion, which usually

took about 4-6 weeks. Sample was washed in 0.2M boric acid and can be left in upon imaging. RapiClear (SunJin lab, RI=1.47) was used for RI matching before imaging.

System PSF characterization. The point spread function of the system was measured by imaging micrometer sized fluorescent beads (17154-10, PolyScience), prepared by a 1:1million dilution in 0.8% low melting agarose solidified in quartz cuvette. The point spread function was imaged by moving the beads in axial direction at 1μm step size. Different number of light sheet lines were used to test the tunable light sheet profiles. For the beads data analysis, images were first processed by ilastik[18] to generate beads mask, which were then used to determine the center of mass coordinates for each bead. Beads from the original image were cropped and aligned based on the center of mass, followed by full width half maximum calculations.

Image processing. Median filter with radius 0.1 was applied to remove hot pixel noise. The image tiles were stitched using terastitcher[19] or bigstitcher[20]. The volume rendering was performed with Amira. For TH segmentation, suiteWB pipeline[17] was used as described previously[17]. Briefly, the whole brain datasets were registered onto a local average reference atlas. The registered data was split into dense and sparse regions for multi-model segmentation. Finally, the detected cells were annotated with Allen brain atlas (ABA, ccfv3) regions for further comparison.

References

1. Stelzer, E. H. K. *et al.* Light sheet fluorescence microscopy. *Nat Rev Methods Primers* **1**, 1–25 (2021).
2. Tomer, R., Ye, L., Hsueh, B. & Deisseroth, K. Advanced CLARITY for rapid and high-resolution imaging of intact tissues. *Nature Protocols* **9**, 1682–1697 (2014).
3. Tomer, R. *et al.* SPED Light Sheet Microscopy: Fast Mapping of Biological System Structure and Function. *Cell* **163**, 1796–1806 (2015).
4. Migliori, B. *et al.* Light sheet theta microscopy for rapid high-resolution imaging of large biological samples. *BMC Biology* **16**, 57 (2018).
5. Dodt, H.-U. *et al.* Ultramicroscopy: three-dimensional visualization of neuronal networks in the whole mouse brain. *Nat Methods* **4**, 331–336 (2007).
6. Glaser, A. K. *et al.* A hybrid open-top light-sheet microscope for versatile multi-scale imaging of cleared tissues. *Nat Methods* **19**, 613–619 (2022).
7. Chen, Y. *et al.* A Versatile Tiling Light Sheet Microscope for Imaging of Cleared Tissues. *Cell Reports* **33**, 108349 (2020).
8. Gao, R. *et al.* Cortical column and whole-brain imaging with molecular contrast and nanoscale resolution. *Science* **363**, eaau8302 (2019).
9. Chakraborty, T. *et al.* Light-sheet microscopy of cleared tissues with isotropic, subcellular resolution. *Nature Methods* **16**, 1109–1113 (2019).
10. Dean, K. M., Roudot, P., Welf, E. S., Danuser, G. & Fiolka, R. Deconvolution-free Subcellular Imaging with Axially Swept Light Sheet Microscopy. *Biophysical Journal* **108**, 2807–2815 (2015).
11. Pitrone, P. G. *et al.* OpenSPIM: an open-access light-sheet microscopy platform. *Nat Methods* **10**, 598–599 (2013).
12. Gualda, E. J. *et al.* OpenSpinMicroscopy: an open-source integrated microscopy platform. *Nat Methods* **10**, 599–600 (2013).

13. Voigt, F. F. *et al.* The mesoSPIM initiative: open-source light-sheet microscopes for imaging cleared tissue. *Nat Methods* **16**, 1105–1108 (2019).
14. Renier, N. *et al.* iDISCO: a simple, rapid method to immunolabel large tissue samples for volume imaging. *Cell* **159**, 896–910 (2014).
15. Chung, K. *et al.* Structural and molecular interrogation of intact biological systems. *Nature* **497**, 332–337 (2013).
16. Kirst, C. *et al.* Mapping the Fine-Scale Organization and Plasticity of the Brain Vasculature. *Cell* **180**, 780-795.e25 (2020).
17. Datta, M. S. *et al.* Whole-brain mapping reveals the divergent impact of ketamine on the dopamine system. 2023.04.12.536506 Preprint at https://doi.org/10.1101/2023.04.12.536506 (2023).
18. Berg, S. *et al.* ilastik: interactive machine learning for (bio)image analysis. *Nat Methods* **16**, 1226–1232 (2019).
19. Bria, A. & Iannello, G. TeraStitcher - A tool for fast automatic 3D-stitching of teravoxel-sized microscopy images. *BMC Bioinformatics* **13**, 316 (2012).
20. Hörl, D. *et al.* BigStitcher: reconstructing high-resolution image datasets of cleared and expanded samples. *Nat Methods* **16**, 870–874 (2019).

Acknowledgements

We are grateful to Roberto Etchenique for initial discussions related to LASER projectors, and thankful to Maura Boldrini for providing fixed human brain tissue sample. This work was supported by NIH grant DP2MH119423 and Columbia University Arts & Sciences startup grant to R.T.

Author Contributions

Y.C. and R.T. conceptualized and designed the project. Y.C. developed the pLSM framework, performed the imaging experiments and analyzed the data. C.G. contributed to the optical simulation, CAD design and generated pLSM renderings. S.C. contributed to initial prototyping and testing. E.D.D. contributed with animal husbandry and general experimental support. M.S.D. generated TH-labelled whole brain samples. R.T. and Y.C. wrote the paper with inputs from all authors. R.T. supervised the project.

Data availability statement

All datasets will be made available on request.

Code availability

All the code is made available publicly as a GitHub repository:

https://github.com/tomerlab/pLSM-Control

Completing interests

Authors declare no competing interests.

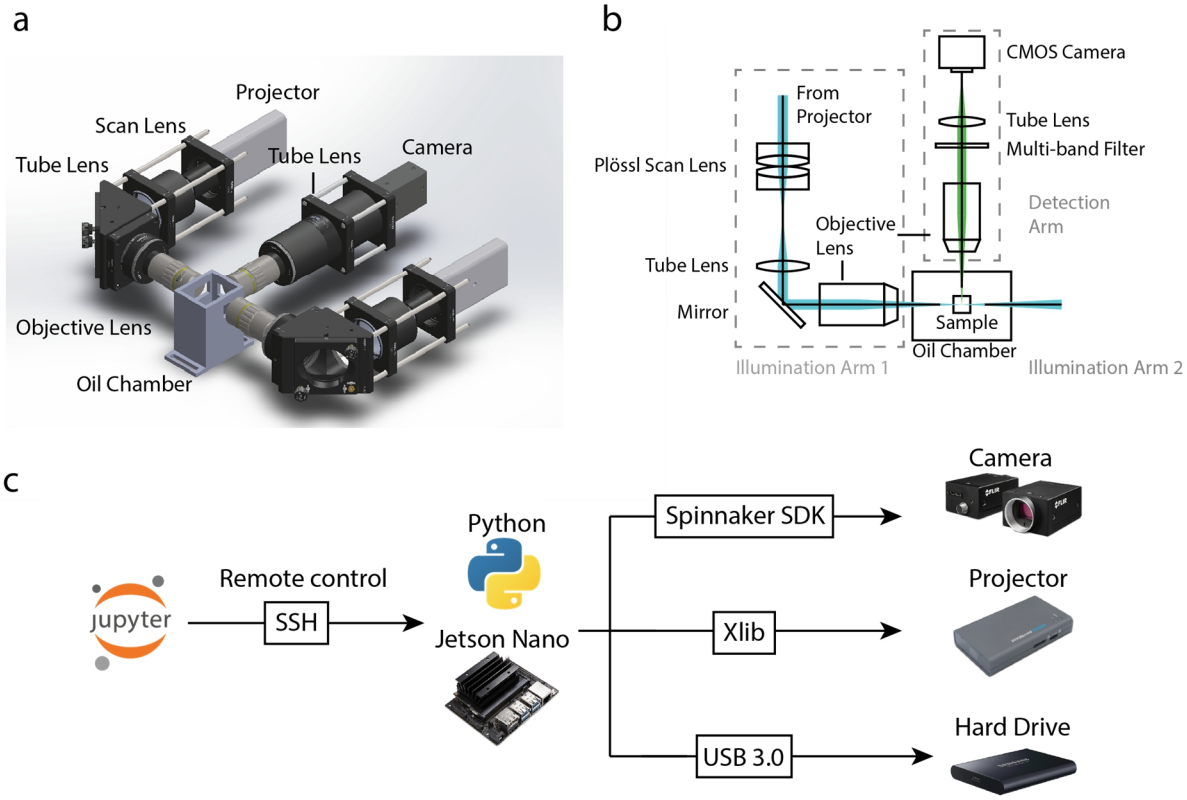

Figure 1. **Implementation of projected Light Sheet Microscopy.** (a-b) 3D model and optical paths of the pLSM system. The pLSM system repurposes pocket LASER projectors for generation of thin scanned light sheets of up to three wavelengths. Two opposing light sheets are employed to illuminate the sample, which is positioned within an oil chamber (the motorized stage holding the sample cuvette is not depicted). The illuminated selective plane is captured by an orthogonally arranged in-focus detection objective, tube lens, and a consumer-grade CMOS camera. (c) The control code, developed using Python, is executed on an Nvidia Jetson Nano board. Remote operation of the system is enabled through a Jupyter Notebook-based graphical user interface (GUI) utilizing the SSH remote protocol. The FLIR CMOS camera is controlled by the Spinnaker SDK package, while the LASER projector via the Xlib library to generate the scanned light sheets. The acquired camera data is streamed to a solid-state hard drive through a high-speed USB 3.0 port.

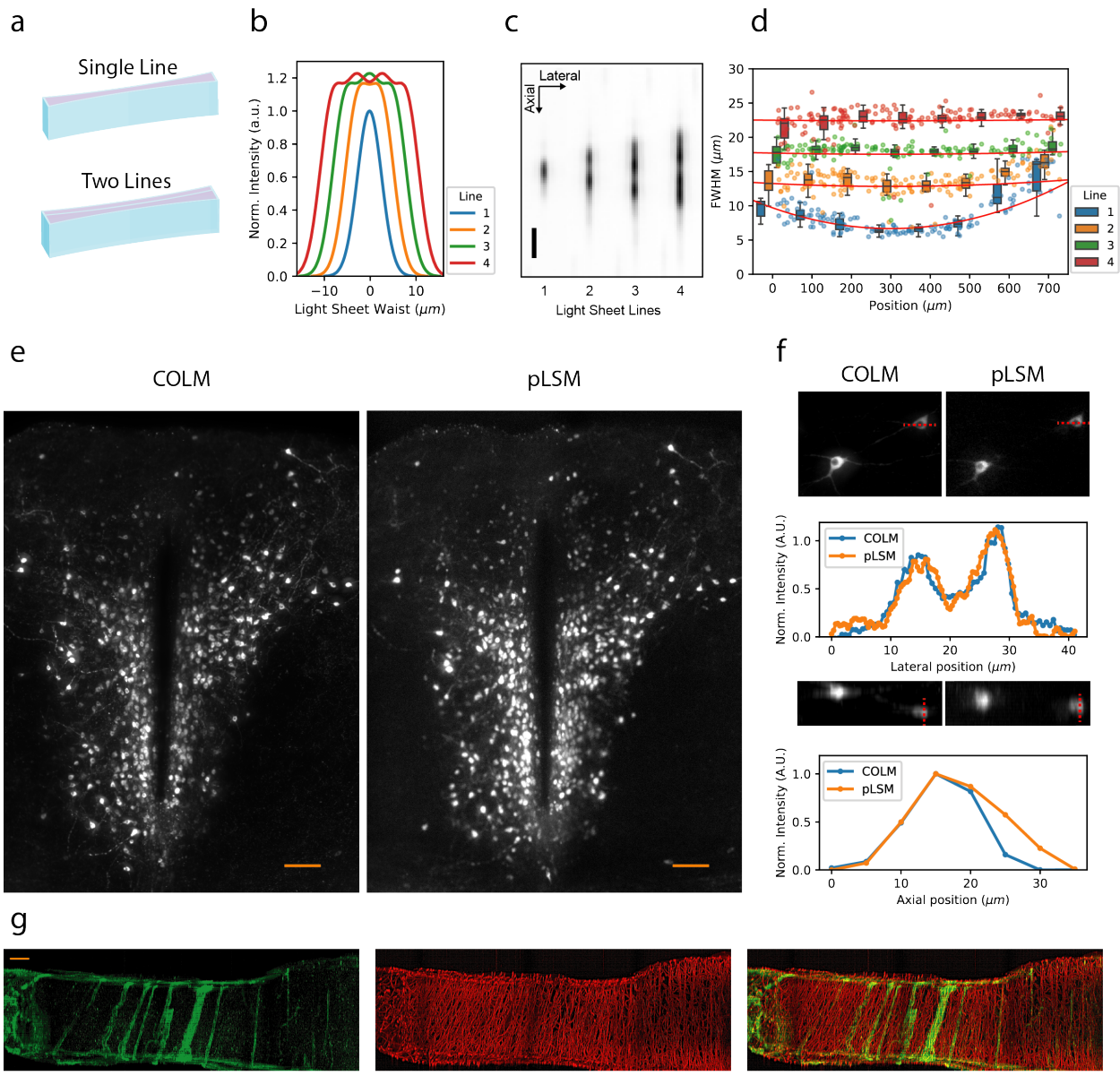

Figure 2. Characterization of projected Light Sheet Microscopy. (a) Schematic illustration demonstrating the generation of light sheets by projecting lines of varying pixel widths (shown for 1- and 2- pixels wide lines). Simulated intensity profiles of the light sheet waist generated by projection of different pixel-width lines. Notably, increasing the number of lines improves the uniformity of the light sheet throughout its cross-section. (c) Measurement of the illumination Point Spread Function (PSF) for the light sheet generated by varying pixel widths. The scale bar represents 10µm. (d) The PSF measurements across the field of view (FOV). In this implementation of pLSM, a single-pixel wide light sheet achieves a thickness of approximately 5 µm at the waist. Light sheets with multiple pixels exhibit greater thickness while achieving significantly improved uniformity across the FOV. (e) Maximum Intensity Projection (MIP) images of TH+ neurons obtained from the same sample using pLSM (with a 2-pixed wide light sheet)

and high-end LSFM implementation COLM. Scale bar represents 100µm. (f) Quantitative analysis and comparison of the intensity profiles of a cell imaged by pLSM and COLM. The pLSM image was preprocessed by applying median filtering (radius=0.1) followed by Gaussian filtering (σ=1) to eliminate hot pixels. (g) Multicolor imaging of human cortex vasculature, stained with Acta2 (AF555, Green) and Podocalyxin/CD31 (AF647, Red). The scale bar represents 200µm.

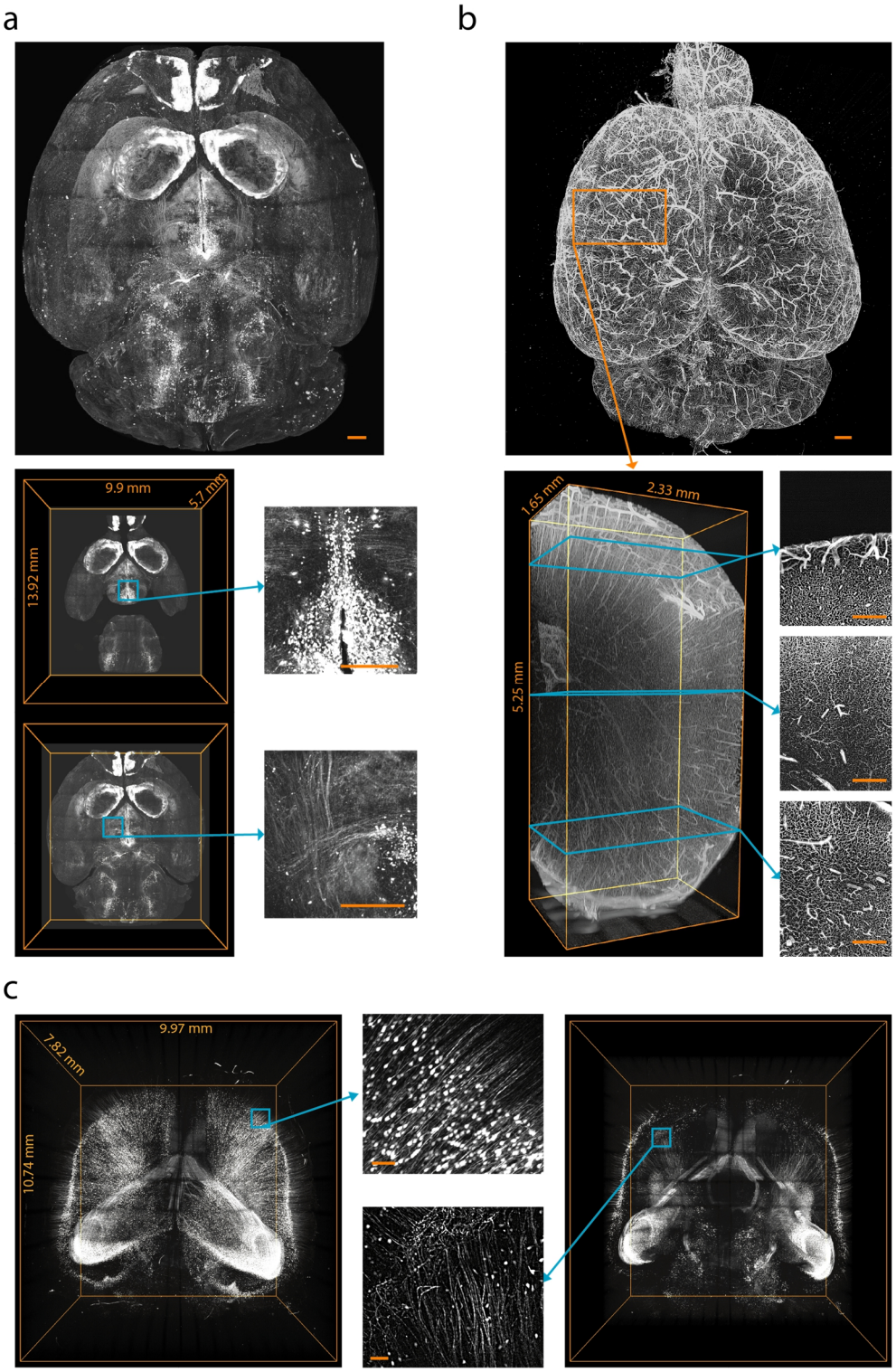

Figure 3. High-resolution pLSM imaging of intact brain samples cleared with iDISCO+ and CLARITY. (a) High-resolution imaging of TH+ dopamine neurons in an iDISCO+ cleared brain sample. The top image presents an overview of the entire brain, while the bottom images provide visualizations of

specific neuronal features at various depths. Scale bars represent 500 µm. Also see **Supplementary Videos 1-2** (b) High-resolution imaging of the complete mouse brain vasculature in an iDISCO+ cleared sample. The top image illustrates the rendering of the entire brain, while the bottom-left image exhibits a 3D rendering of a smaller volume. Additionally, 100µm thickness Maximum Intensity Projections (MIPs) are depicted at different imaging depths. Scale bars represent 500 µm. (c) High-resolution imaging of an intact Thy1-eYFP mouse brain cleared through passive CLARITY. The left image presents the rendering of the whole brain, while the right image shows a 3D rendering of the deeper half of the brain. Also see **Supplementary Video 3**. Scale bars represent 100 µm.

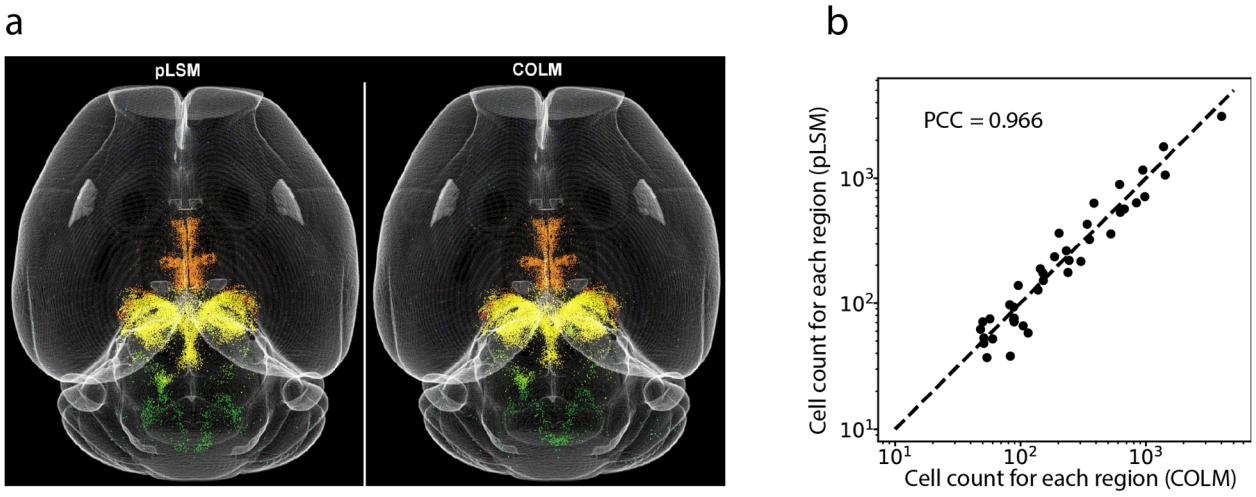

Figure 4. Quantitative assessment of whole brain images obtained through projected Light Sheet Microscopy. (a) Segmentation of TH+ dopamine neurons in datasets acquired by pLSM and COLM imaging of the same sample. The point clouds are color-coded according to the regional annotations from the Allen Brain Atlas at level 8. (b) Comparative analysis of region-specific neuron counts extracted from pLSM and COLM images. The top 40 regions were included in the analysis. The Pearson correlation coefficient of 0.966 indicates a high degree of agreement between the two imaging methods.